Clim Dyn (2016) 46:865–877
DOI 10.1007/s00382-015-2618-x

Effects of tropical North Atlantic SST on tropical cyclone genesis in the western North Pacific

Jinhua Yu[1] · Tim Li[1,2] · Zhemin Tan[3] · Zhiwei Zhu[1,2]

Received: 19 July 2014 / Accepted: 12 April 2015 / Published online: 23 April 2015

Abstract The tropical cyclone genesis number (TCGN) in July–October (JASO) over the western North Pacific (WNP) exhibits a robust interannual variation. It shows a longitudinally tri-pole pattern with a high in the eastern WNP and South China Sea (SCS) and a low in the western WNP, which explain 42.2 and 23.4 % of total TCGN variance in the eastern WNP and SCS, respectively. The high–low–high pattern is similar to that derived from a TC genesis potential index (GPI). To understand the cause of the longitudinal distribution of the dominant interannual mode, we examine the contributions of environmental parameters associated with GPI. It is found that relative humidity and relative vorticity are important factors responsible for TC variability in the SCS, while vertical shear and relative vorticity are crucial in determining TC activity in eastern WNP. A simultaneous correlation analysis shows that the WNP TCGN in JASO is significantly negatively correlated (with a correlation coefficient of −0.5) with sea surface temperature anomalies (SSTA) in the tropical North Atlantic (TNA). The longitudinal distribution of TC genesis frequency regressed onto TNA SSTA resembles that regressed upon the WNP TCGN series. The spatial patterns of regressed environmental variables onto the SSTA over the TNA also resemble those onto TCGN in the WNP, that is, an increase of relative humidity in the SCS and a weakening of vertical shear in the eastern WNP are all associated with cold SSTA in the TNA. Further analyses show that the cold SSTA in the TNA induce a negative heating in situ. In response to this negative heating, a low (upper)-level anomalous aniti-cyclonic (cyclonic) flows appear over the subtropical North Atlantic and eastern North Pacific, and to east of the cold SSTA, anomalous low-level westerlies appear in the tropical Indian Ocean. Given pronounced mean westerlies in northern Indian Ocean in boreal summer, the anomalous westerly flows increase local surface wind speed and surface evaporation and cool the SST in situ. Cold SSTA in northern Indian Ocean further suppress local convection, inducing anomalous westerlies to its east, leading to enhanced cyclonic vorticity and low surface pressure over the WNP monsoon trough region. Idealized numerical experiments further confirm this Indian Ocean relaying effect, through which cold SSTA in the tropical Atlantic exert a remote impact to circulation in the WNP.

Keywords Tropical North Atlantic SST · Tropical cyclone genesis in the western North Pacific · Teleconnection

1 Introduction

The western North Pacific (WNP) is the most frequent tropical cyclone (TC) genesis region in the globe. The summer mean circulation in the WNP has some unique features. For example, the WNP is the region of the greatest warm pool in boreal summer, with averaged sea surface temperature (SST) >29 °C. The low-level circulation is characterized by a confluent zone between the monsoon westerlies and the trade easterlies. The low-level convergence zone overlaps

✉ Tim Li
timli@hawaii.edu

[1] CDRC/ESMC, International Laboratory on Climate and Environment Change, Nanjing University of Information Science and Technology, Nanjing 210044, China

[2] IPRC and Department of Atmospheric Sciences, University of Hawaii, Honolulu, HI 96822, USA

[3] Key Laboratory of Mesoscale Severe Weather/Ministry of Education, Nanjing University, Nanjing 210093, China

with maximum cyclonic vorticity and deep convection, forming the WNP monsoon trough under which many perturbations grow. The mean flow feature differs distinctively from that in the North Atlantic (NA, Peng et al. 2012, Fu et al. 2012), where there is no monsoon trough. In addition to the mean flow, perturbation types that trigger cyclogenesis are also different between the two basins. In NA major perturbations are African easterly waves, whereas in WNP precursor perturbations include TC energy dispersion induced Rossby wave trains (Li and Fu 2006), northwest–southeast oriented synoptic wave trains (Lau and Lau 1990, Li 2006), and Pacific easterly waves (Fu et al. 2007).

In addition to a marked annual cycle, TC genesis number (TCGN) in the WNP basin experiences a strong interannual variation (Wang and Chan 2002; Chen et al. 2006). Many previous studies focused on the interannual variation of TCGN in the WNP during TC peak season (July–October) in relation with ENSO. There is a general consensus that ENSO affects the location of TC formation in the WNP. However, the coefficient between total genesis number in the WNP and ENSO index is statistically insignificant (Chia and Ropelewski 2002; Lander 1993; Li 2012). A significant correlation was only found when separating El Niño into developing and decaying phases in TC season from May to October (Du et al. 2011; Li 2012). It has been shown that during the El Niño developing phase, TC genesis location is shifted more to the southeastern quadrant of the WNP basin (Chan 2000; Wang and Chan 2002; Chen et al. 2006; Frank and Young 2007), even though total TC number undergoes little change. A significant decrease of TCGN occurred in the WNP during the El Nino decaying summer (when the Niño indices are about normal). The marked reduction of TCGN during the El Niño decaying summer is primarily attributed to the weakening of the WNP monsoon, which is caused by both the local air-sea interaction (Wang and Li 2003) and remote SST forcing from the tropical Indian Ocean (Wu et al. 2009, 2010; Du et al. 2011).

Most of the previous studies focused on the role of the sea surface temperature anomalies (SSTA) in the tropical Pacific (e.g., Wang and Chan 2002) and Indian Ocean (Zhan et al. 2011), less attention is paid on the effect of the Atlantic SST on the WNP TCs. On a longer timescale, it has been shown that the Atlantic Multi-decadal Oscillation (AMO) (Kushnir 1994; Sutton and Hodson 2005) may exert a remote forcing onto the tropical Pacific. This teleconnection process is transmitted through either an atmospheric bridge (Dong and Sutton 2007) or the global oceanic wave adjustment (Timmermann et al. 2005). For example, Timmermann et al. (2005, see their Fig. 1) suggested that Kelvin waves triggered by a density perturbation in the Atlantic may propagate around African Coast via the form of coastal Kelvin waves and then propagate across the

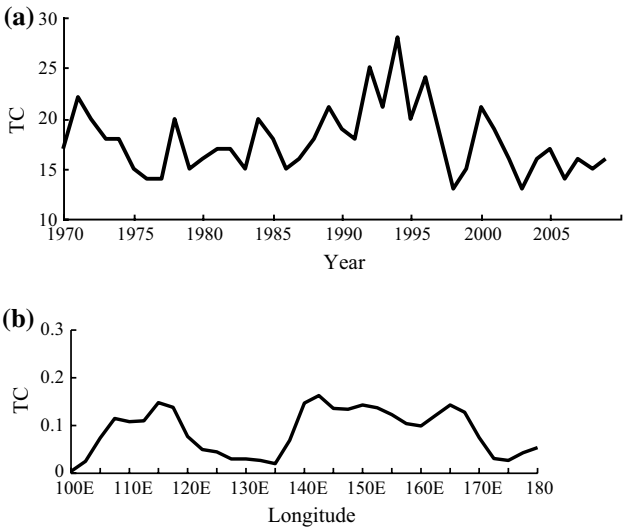

Fig. 1 **a** Time series of TCGN in the WNP during JASO and **b** longitudinal distribution of regressed TCGN between 10°–25°N at each 2.5 longitude upon the total TCGN series shown in Fig. 1a. *Regressed coefficients* (unit: TC) shown in Fig. 1b represent TCGN variation in each longitude per standard deviation of the total TCGN

equatorial Indian Ocean and Maritime Continent/Australia via the form of equatorial/coastal Kelvin waves. A few of recent studies suggested some mechanisms about the influence of the Atlantic SSTA on El Niño/La Niña event. For example, Wang et al. (2011) suggested that the response to the SSTA in the North Atlantic is likely to be conveyed through the Eurasian Continent via the East Atlantic (EA)/West Russia (WR) teleconnection pattern. Ding et al. (2012) and Ham et al. (2013) suggested that the positive tropical Atlantic SSTA might induce a La Niña event through induced tropical or subtropical wind anomalies in the eastern Pacific. Rong et al. (2010) showed that the SSTA in the tropical Atlantic can affect the WNP monsoon through induced equatorial Kelvin waves that spread from the source region into the tropical Indian Ocean and western Pacific. The atmospheric response to SSTA in tropical North Atlantic (TNA) appears strongest in boreal summer (Sutton and Hodson 2007).

The objective of this study is to reveal the role of the Atlantic SSTA in causing the interannual variation of TCGN in the WNP during the TC peak season (July–October). As we will demonstrate, maximum simultaneous correlation between the TCGN in the WNP and SSTA occurs in the TNA, not in the western Pacific or Indian Ocean. Given such an observed feature, we further investigate mechanisms through which the Atlantic SSTA affects the WNP TCGN. For the dominant interannual mode of the WNP TCGN, a particular focus is on its longitudinal distribution and the relative contribution of environmental parameters to such a distribution. The remaining part of the

paper is organized as follows. In Sect. 2 we introduce the dataset and methodology used. Section 3 analyzes the longitudinal distribution of the dominant interannual mode of WNP TCGN and the relative role of environmental parameters in determining the longitudinal distribution of the dominant TCGN mode. The relationship between the interannual variation of TCGN in the WNP and global SSTA is presented in Sect. 4. In Sect. 5 we propose possible mechanisms through which SST anomalies in the tropical Atlantic affect the TC activity in the WNP. Finally, a summary and discussion are given in Sect. 6.

2 Data and methodology

2.1 Observational data

Six-hourly TC best track data over the WNP (0°–40°N, 100°E–180°, including the western North Pacific and the South China Sea) are obtained from the Joint Typhoon Warning Center (JTWC, downloaded from http://www.usno.navy.mil/NOOC/nmfc-ph/RSS/jtwc/best_tracks/). The analyses will cover a 40-year period from 1970 to 2009, given that the base track data are much more reliable after 1970 when satellite observations became available (Zhao et al. 2014). To minimize the subjectivity in identifying weak systems, only TCs that reach tropical storm intensity (with maximum sustained 1-m winds reaching 17.2 m s^{-1}) or above are included in the analyses. TC genesis frequency in the WNP shows a pronounced annual cycle with a peak in August. The current analyses will focus on the peak TC season from July to October (JASO), in which about 70 % of the total TCs occur.

Monthly mean SST data are from the Hadley Centre interpolated SST dataset with 1° spatial resolution (HadISST1; Rayner et al. 2003). All monthly mean atmospheric data are derived from the National Centers for Environmental Prediction (NCEP)/National Center for Atmospheric Research (NCAR) reanalysis (Kalnay et al. 1996), which has a horizontal resolution of 2.5° longitudes by 2.5° latitudes at 17 (8 for humidity) pressure levels. NOAA monthly mean outgoing long-wave radiation (OLR) during 1974–2009 is used to represent large-scale convective heating in the tropics. The linear trends of TCGN and other variables are removed prior to the analyses.

2.2 Methodology

The genesis potential index (GPI) developed by Emanuel and Nolan (2004) has been widely used to estimate the model TCGN based on large-scale dynamic and thermodynamic fields (e.g., Camargo et al. 2007, 2009). To quantitatively assess the relative contributions of different environmental parameters, we follow a partial derivative method developed by Camargo et al. (2007) and Li et al. (2013). The GPI may be written as.

$$GPI = Term1 \times Term2 \times Term3 \times Term4, \tag{1}$$

where $Term1 = |10^5\eta|^{3/2}$, $Term2 = (\mathrm{H}/50)^3$, $Term3 = (\mathrm{Vpot}/70)^3$, $Term4 = (1 + 0.1\mathrm{Vshear})^{-2}$, η is the absolute vorticity at 850 hPa (in 10^{-5} s^{-1}), H is the relative humidity at 600 hPa in percent, V_{pot} is the TC maximum potential intensity (in m s^{-1}) defined by Emanuel (1987, 1988),

$$V_{pot} = \sqrt{\frac{T_S}{T_0}\frac{C_k}{C_D}[CAPE^* - CAPE]_m} \tag{2}$$

where T_s is the SST; T_0 is the outflow layer temperature; C_k is the exchange coefficient for enthalpy; C_D the drag coefficient; here we take $\frac{C_k}{C_D} = 0.8$. $CAPE^*$ is the convective available potential energy of air saturated at SST and lifted from sea level in reference to the environmental sounding, and $CAPE$ is that of boundary layer air. The subscript "m" indicates the values evaluated near the radius of maximum wind. V_{shear} is the magnitude of the vertical wind shear between 850 and 200 hPa (in m s^{-1}).

Following Li et al. (2013), the relative contributions of each individual term to the total GPI change may be written as

$$\delta GPI = \alpha_1\delta Term1 + \alpha_2\delta Term2 + \alpha_3\delta Term3 + \alpha_4\delta Term4 \tag{3}$$

where coefficients α_1, α_2, α_3 and α_4 may be approximately determined based on the following method:

$$\alpha_1 = \overline{Term2 \cdot Term3 \cdot Term4}$$
$$\alpha_2 = \overline{Term1 \cdot Term3 \cdot Term4}$$
$$\alpha_3 = \overline{Term1 \cdot Term2 \cdot Term4}$$
$$\alpha_4 = \overline{Term1 \cdot Term2 \cdot Term3}$$

In the equation above, a bar denotes a time average for JASO in 1970–2009. The term with δ can be its anomaly or regression value.

2.3 Model

The atmospheric general circulation model (GCM) used in this study is the ECHAM4 (Roesch et al. 2001), which employs a spectral dynamic core. We use a version with triangular truncation at zonal wavenumber 42 (T42; equivalent to 2.85° horizontal resolution) and 19 sigma levels in the vertical.

The ECHAM4 is forced with the observed monthly climatology of SST and sea ice. A 20-year run with this SST forcing is regarded as a control simulation. We conducted two sets of sensitivity experiments. In the first set, we specify the regressed SSTA patterns in the TNA (0–30°N, 80°W–0°) and/or the tropical Indian Ocean (TIO, 20°S–20°N, 40°–90°E). In the second set, an idealized (ellipse shape) SSTA pattern with the amplitude of the SSTA magnified (twice as large as the regressed) is specified in the two basins. Each set includes three experiments: SST anomalies are confined in TNA, TIO, and both TNA and TIO, respectively.

3 Longitudinal distribution of the WNP dominant interannual TCGN mode

Figure 1a shows the time series of TCGN in JASO over the WNP from 1970 to 2009. It exhibits a marked interannual variation. The average number is 17.8 TC year^{-1}. During the 40-year period, the TCGN in the WNP does not show a significant long-term trend. In fact, the linear trend only contributes 0.5 % to the total variance.

To examine the longitudinal distribution of the dominant interannual mode of TCGN in the WNP, we calculated the longitudinal pattern of TC genesis frequency in the band of 10°–25°N regressed against the time series shown in Fig. 1a, and the regression coefficients (indicating the TCGN variation in each longitude per standard deviation of the total TCGN) are shown in Fig. 1b. It is interesting to note that there is a marked longitudinal variation, with two peaks in 110°–120°E and 140°–170°E and a low in 120°–140°E. This implies that during a high TCGN year, majority of TC genesis occurs over the South China Sea (SCS, 100°–120°E) and the eastern WNP (EWNP, 140°E–180°) while there is much less TC activity over the western WNP (WWNP, 120°–140°E). The regressed regional TCGNs over the SCS and EWNP explain 23.4 and 42.2 % of total TC variance at a 99 % confidence level, respectively. The regressed TCGN over the WWNP, on the other hand, explains only a very small portion of total variance and is not statistically significant.

A natural question is what causes the longitudinal distribution of interannual TCGN variability in the WNP. Changes in TC genesis frequency are closely related to changes in the large-scale environmental variables such as SST, relative humidity in the mid troposphere (e.g., at 600 hPa), relative vorticity in the lower troposphere (e.g., at 850 hPa), potential intensity and the magnitude of vertical wind shear between 200 and 850 hPa. So far a few TC genesis indices have been suggested based on above environmental parameters (e.g., Gray 1968; Royer et al. 1998; Emanuel and Nolan 2004). While these indices are in general good in reproducing the annual cycle of TC number in different basins (Menkes et al. 2012), they have less capability in capturing interannual TC variability. Among them, the GPI of Emanuel and Nolan (2004) is used most widely. Camargo et al. (2007) showed that this index did a good job in reproducing TC variability linked to ENSO. Because of that, in the current analysis we use this index. We calculated box-averaged GPIs against the time series of TCGN over the WNP during JASO (shown in Fig. 1a) for the three regions (SCS, WWNP and EWNP). They reflect the interannual variation of regional GPI associated with the TCGN over the WNP. As shown by red bars in Fig. 2, the GPIs well capture the longitudinal distribution of the dominant TCGN mode with positive GPI anomalies in EWNP and SCS and negative GPI anomalies in WWNP.

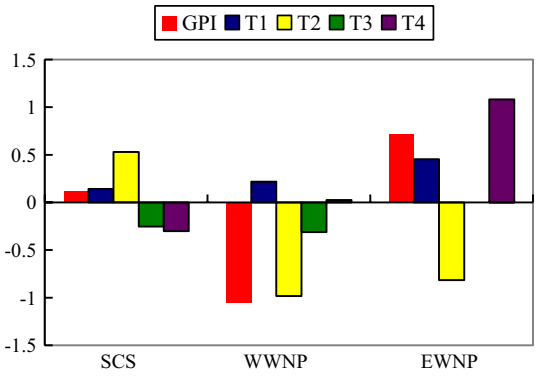

Fig. 2 Regional GPI regressions onto total TCGN in the WNP and the relative contributions to the GPI changes of four environmental parameter terms, α_1 δTerm1 (denoted as *T1*), α_2 δTerm2 (denoted as *T2*), α_3 δTerm3 (denoted as *T3*) and α_4 δTerm4 (denoted as *T4*) averaged over SCS (100°–120°E, 10°–25°N), WWNP (120°–140°E, 10°–25°N) and EWNP (140°–170°E, 10°–25°N)

The relative contributions of different terms to the GPI changes were computed based on Eq. (3) and the results are shown in Fig. 2. Note that the contributions of the four terms to the GPI changes differ among three sub-regions.

Table 1 Area-averaged value of δGPI and four environmental terms in three sub-regions, SCS, WWNP and EWNP, regressed against the TCGN time series in Fig. 1a

Area	δGPI	α_1δTerm1	α_2δTerm2	α_3δTerm3	α_4δTerm4
SCS	0.12	0.14 (+116 %)	0.53 (+441 %)	−0.25 (−208 %)	−0.3 (−250 %)
WWNP	−1.05	0.22 (−21 %)	−0.98 (+93 %)	−0.31 (+30 %)	0.02 (−2 %)
EWNP	0.72	0.45 (+63 %)	−0.82 (−114 %)	0.00 (0 %)	1.08 (150 %)

Number in bracket denotes the percentage contribution of each term to the GPI change at each sub-region

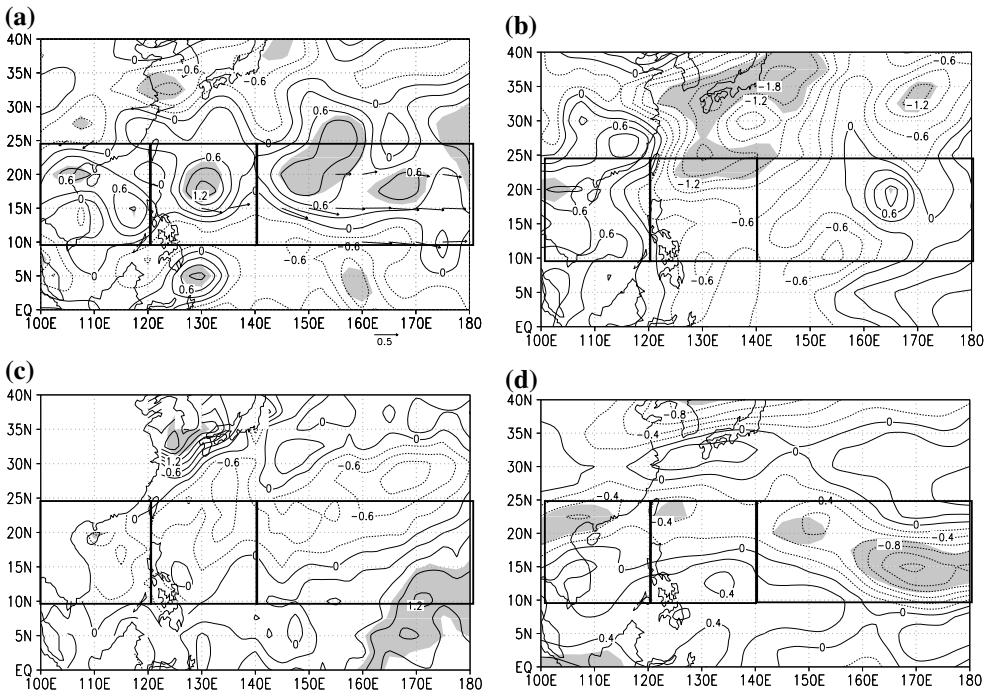

Fig. 3 Horizontal distribution of **a** regressed relative vorticity (unit: 10^{-6} s^{-1}) and wind vector (unit: ms^{-1}, only the values at the 95 % confidence level or higher are shown) at 850 hPa, **b** relative humidity at 600 hPa (unit: %), **c** potential intensity (ms^{-1}) and **d** vertical wind shear (unit: ms^{-1}) against the TCGN series shown in Fig. 1a. The *shading region* is at 95 % confidence level or higher for contour. *Rectangles* from *left* to *right* represent SCS, WWNP and EWNP regions

The first term $\alpha_1\delta Term1$ (which is associated with environmental absolute vorticity at 850 hPa) is all positive across all three areas, with the largest value in EWNP. The second term $\alpha_2\delta Term2$ (which is associated with environmental relative humidity) is positive in SCS but negative in other two areas. The third term $\alpha_3\delta Term3$ (which is associated with the environmental potential intensity) is negative in SCS and WWNP and near zero in EWNP. The fourth term $\alpha_4\delta Term4$ (which is related to the environmental vertical shear effect) exhibits a large positive value in EWNP, a negative one in SCS and near zero in WWNP.

Table 1 shows the quantitative assessment of the four terms that contribute to the GPI changes over the three sub-regions. In EWNP, the GPI increase (+0.72) is attributed to the net effect of environmental vertical wind shear (contribution to GPI change: +1.08) and absolute vorticity (contribution to GPI change: 0.45) that overwhelm the environmental water vapor effect (contribution to GPI change: −0.82). This result is consistent with Liu and Chan (2013), who found that enhanced vertical wind shear is responsible for decreased TC frequency in the eastern part of the tropical WNP during a TC inactive period. Here we provide a quantitative assessment, that is, even though the vertical wind shear plays an important role, it alone is not enough. The vertical shear needs to work together with absolute vorticity to overcome the humidity effect.

A large decrease of GPI (−1.05) occurs in WWNP. The key process responsible for such a large negative value is attributed to the decrease of the mid-level atmospheric relative humidity. This environmental factor plays a dominant role in the region and it alone counts for 93 % of the total decrease of GPI (Table 1). This is consistent with Camargo et al. (2007), who found that diminished relative humidity is responsible for decreased TC frequency in the western part of the tropical WNP during El Niño. The environmental absolute vorticity (+0.22) is approximately compensated by the potential intensity effect (−0.31) in the region. In contrast to EWNP, the vertical wind shear in WWNP has little effect to the change of GPI.

The increase of GPI (+0.12) in SCS is primarily attributed to the effects of atmospheric relative humidity (contribution to GPI change: +0.53) and absolute vorticity (contribution to GPI change: +0.14), while both the potential intensity (contribution to GPI change: −0.25) and vertical wind shear (contribution to GPI change: −0.3) have an opposite effect. The result indicates that the environmental relative humidity plays a dominant role in causing the interannual variability of TC genesis frequency in SCS.

The diagnosis result above is consistent with the longitudinal distribution of regressed individual fields as shown in Fig. 3. In the band of 10°–25°N, cyclonic vorticity anomalies dominate over all three WNP sub-regions. The relative

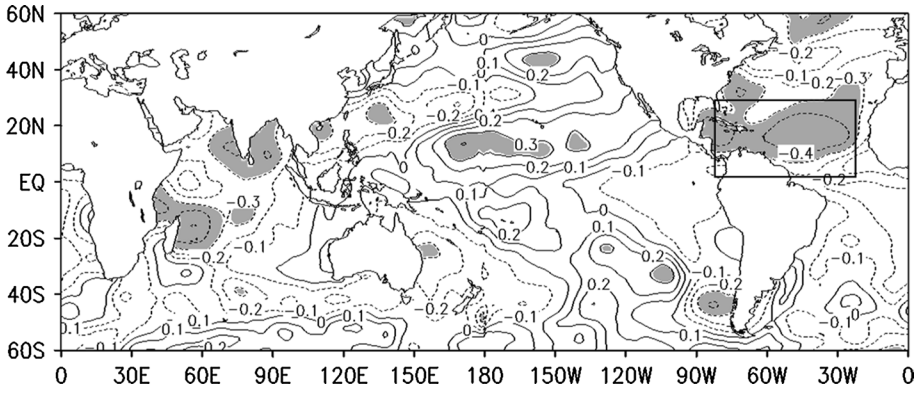

Fig. 4 Spatial distribution of correlation coefficients between TC genesis frequency in the WNP and SSTA in 60°S–60°N during JASO. The *shadings* indicate the correlation coefficients significant at a 0.05 significance level, the square (80°–20°W, 5°–30°N) is a selected region with significant correlation, where SST averaged indicate an index of tropical North Atlantic

humidity has a positive anomaly over SCS and in far eastern WNP and a negative anomaly in between. Only the region near SCS exceeds 0.05 significant level. The potential intensity has overall negative values, implying that this environmental factor tends to prevent cyclogenesis in almost all WNP region. However, the influence of potential intensity is weak, which is consistent with previous studies (Wang and Chan 2002; Camargo et al. 2007). Indeed, the potential intensity reflects effects of SST and Wang and Chan (2002) suggested that there is almost no relationship between local SST and TC genesis over the WNP. The vertical shear field shows a large negative center in EWNP (which exceeds 0.05 significant level), indicating a marked reduction of background vertical wind shear there.

To summarize, the overall contribution to the high–low–high longitudinal distribution shown in Fig. 1b arises from environmental relative humidity and vertical shear. A dominant factor that contributes to a positive (negative) GPI in SCS (WWNP) is the relative humidity, whereas a dominant factor that contributes to a positive GPI in EWNP is the vertical shear.

4 Relationship between anomalous TCGN in the WNP and global SSTA

The El Niño-South Oscillation (ENSO) is a major driver of climate variability on interannual time scales, but the simultaneous correlation between TCGN in the WNP and ENSO indices is low (Li 2012). This motivates us to examine the simultaneous correlations between the TCGN in JASO and the global SSTA to find out key regions where the SSTA may be significantly correlated with TC genesis frequency over the WNP.

Figure 4 shows the distribution of the simultaneous correlation coefficient between the TCGN over the WNP and the global SSTA in JASO (with a linear trend removed). It is interesting to note that the largest region with significant negative correlations that exceed a 95 % confidence level appears in the TNA around 80°–20°W, 5°–30°N. A smaller

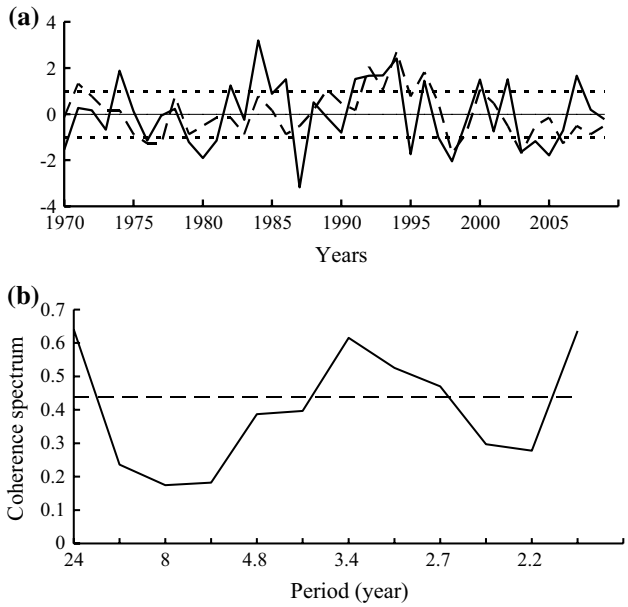

Fig. 5 **a** Time series of normalized TNAI (*solid line*) and TCGN in the WNP (*dashed line*), the *dot lines* are the value of 1 and −1, respectively; **b** coherence spectrum between the TCGN and TNAI time series. *Dashed line* in (**b**) denotes a 95 % confidence level

region with also a significant negative correlation appears over the tropical Indian Ocean. A weak dipole correlation pattern occurs in the tropical WNP.

To investigate the relationship between TC activity in the WNP and TNA SST anomalies, we constructed a tropical North Atlantic Index (TNAI) by averaging SSTA over 5°–30°N, 80°–20°W during JASO and multiplying −1 to the averaged SSTA. Adding a negative sign is to reflect the negative correlation between TCGN and SSTA in TNA, so that a positive value of TNAI corresponds to the increase of TCGN in the WNP.

Figure 5a shows normalized TNAI and TCGN time series. The correlation coefficient between the two time series is 0.50, exceeding a 99 % confidence level. In the following we will conduct both the regressed and composite

analyses. For the composite analysis, the high (low) cases are defined when TNAI exceeds one (negative one) standard deviation. Twelve high TNAI years were selected in total: 1974, 1982, 1984, 1986, 1991, 1992, 1993, 1994, 1996, 2000, 2002 and 2007. Twelve low TNAI years were selected in total: 1970, 1976, 1979, 1980, 1981, 1987, 1995, 1997, 1998, 2003, 2004, and 2005. The averaged TCGN during JASO in the high (low) TNAI years is 21.3 (15.8) over the WNP. The average difference, between the high and low TNAI years is 5.5 TC year^{-1} which is significant at a 0.05 significant level, implying that a cold tropical North Atlantic Ocean favors more frequent TC genesis over the WNP.

A cross spectrum analysis shows that the dominant coherence periodicity between the TCGN and TNAI appears in the interannual band (Fig. 5b). The most significant peak for both the indices appears at about 3 years, which exceeds a 95 % confidence level. This timescale is essentially of ENSO frequency, which may be related to some 6-month delayed influence of ENSO as will be discussed in Sect. 6. The significant correlation and the coherence spectrum peaks between the TCGN and TNAI give us confidence to further investigate the effect of TNA SSTA on the TC activity in the WNP.

We first examine the longitudinal distribution of regressed TC frequency against the TNAI time series. The corresponding longitudinal pattern (solid curve in Fig. 6, regression coefficients represent the TCGN variation in each longitude per standard deviation of the TNAI series) in the band of 10°–25°N in general resembles that shown in Fig. 1b except for a relatively large difference between 135°E and 145°E. The difference between solid and dashed curves implies that other factors (e.g., land-sea thermal contrast, higher-frequency variability) besides the SSTA may influence the longitudinal distribution of TCGN. We also calculated the relative contributions of four environmental parameter terms to the GPI changes regressed against the TNAI time series. The overall result (not shown) is quite similar to Fig. 2.

Next we examine the patterns of environmental vorticity, relative humidity, potential intensity and vertical shear regressed against the TNAI series (Fig. 7). It is interesting to note that in association with a high TNAI or cold SSTA over the TNA, cyclonic vorticity anomalies appear over most of the WNP cyclogenesis region. The relative humidity field is dominated by a high–low–high pattern, with an increase (decrease) of relative humidity in SCS and EWNP (WWNP). The potential intensity has overall negative values in the WNP. As shown in next section, this feature is consistent with the regressed SST pattern, which shows dominant local negative SST anomalies in the region. In most of the regions, the regressed potential intensity field does not exceed a 95 % confidence level. The vertical shear

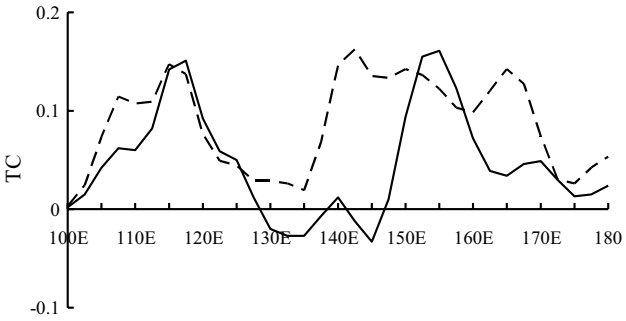

Fig. 6 Longitudinal distribution of TC genesis frequency in the band of 10°–25°N regressed against the TNAI series (*solid line*). *Regressed coefficients* (unit: TC) represent TCGN variation in each longitude per standard deviation of the TNAI. For comparison, the longitudinal distribution regressed against the TCGN series is also plotted here (*dashed line* same as that shown in Fig. 1b)

field shows an east–west asymmetry, with reduced vertical shear in EWNP (exceeding a 95 % confidence level). The spatial patterns of the environmental variables regressed on TNAI resemble those regressed on TCGN shown in Fig. 3. A pattern correlation coefficient between relative vorticity at 850 hPa, relative humidity at 600 hPa, potential intensity and vertical shear in Figs. 3 and 7 are 0.65, 0.74, 0.77 and 0.77, respectively.

The analysis above suggests that the tropical Atlantic SSTA may remotely affect the TC activity over the WNP through the change of environmental vorticity, vertical wind shear and relative humidity. In the next section we will investigate possible processes through which the tropical Atlantic Ocean remotely affects circulation in the WNP.

5 Processes through which tropical Atlantic SSTA affect TCs in the WNP

To examine specific processes through which the tropical Atlantic SST anomalies influence western North Pacific TC activity, we first conducted a regression analysis against the TNAI time series. We made regressions of atmospheric and oceanic variables against the TNAI series during JASO to indentify the processes linking negative SSTA in the TNA and the TCGN variation over the WNP. The regressed results reflect atmospheric and oceanic responses to the negative SSTA in the TNA.

Figure 8 shows the SST and OLR anomalous patterns regressed upon the TNAI time series during JASO. As expected, the TNA is characterized by large-scale negative SSTA. It is interesting to note that there are significant negative SSTA in the North Indian Ocean (NIO). Accompanied with the negative SSTA over the TNA and NIO, there are suppressed convective activity with the large positive OLR

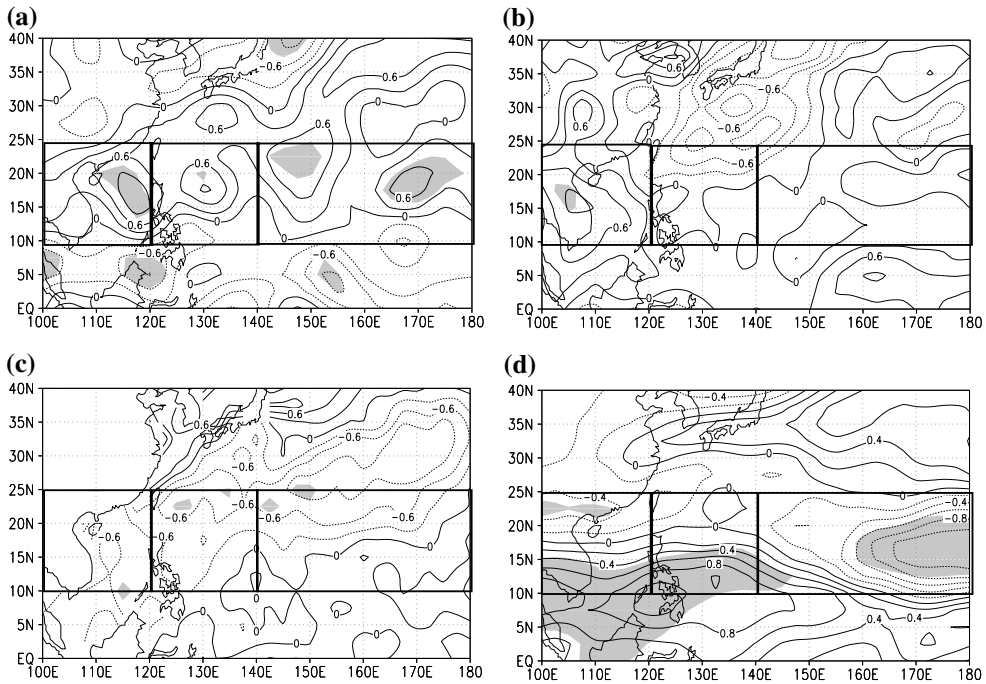

Fig. 7 Same as Fig. 3 except for regression on the TNAI series during JASO

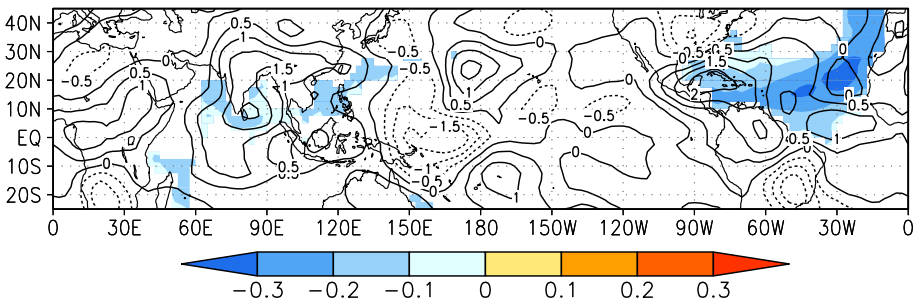

Fig. 8 Regressed SST (*shading*, unit: °C, only the values at the 95 % confidence level or higher are shown) and OLR (contour, unit: Wm^{-2}) in 1974–2009 against the TNAI during JASO

anomalies. This indicates that in both the regions it is the ocean that drives the atmosphere. Then a question arises as what causes the cooling in northern Indian Ocean?

We hypothesize that the cooling in NIO is a result of TNA SSTA forcing. The cooling associated with weaker convection in TNA leads a low-level anticyclonic flow (Fig. 9a) and an upper-level cyclonic flow (Fig. 9b) over the subtropical North Atlantic and eastern Pacific. Meanwhile, westerly wind anomalies to the east of TNA are generated as a Gill-type Kelvin wave response to the anomalous negative heating (Gill 1980). Given pronounced mean westerlies in NIO in boreal summer, anomalous westerly flows in response to the Atlantic cold SSTA may increase the local surface wind speed and thus surface evaporation and vertical ocean mixing, which cool the SST in situ. The connection between the tropical Atlantic and Indian Ocean is supported by coupled ocean–atmosphere model experiments of Wang et al. (2009), who investigated the response of the Indian Ocean SSTA to the tropical Atlantic SSTA forcing in JJAS and found that warm SSTA were induced in the tropical Indian Ocean due to decreased evaporation in response to warm SSTA forcing over the tropical Atlantic.

What is the effect of the NIO SSTA in connecting the Atlantic SSTA and circulation anomalies in the WNP? The cold SSTA in NIO may further suppress local convection, inducing anomalous low-level westerly to its east. The enhanced westerlies in the WNP monsoon trough region can further strengthen the low-level cyclonic vorticity and boundary-layer moisture convergence, leading to a stronger monsoon. Through this Indian Ocean relaying effect, the tropical Atlantic SSTA may exert a remote impact to the mean monsoon circulation and thus TC activity in the WNP.

One may wonder whether it is possible that TNA SSTA can exert a remote forcing effect all the way to the western Pacific without the help of the NIO SSTA. To address this

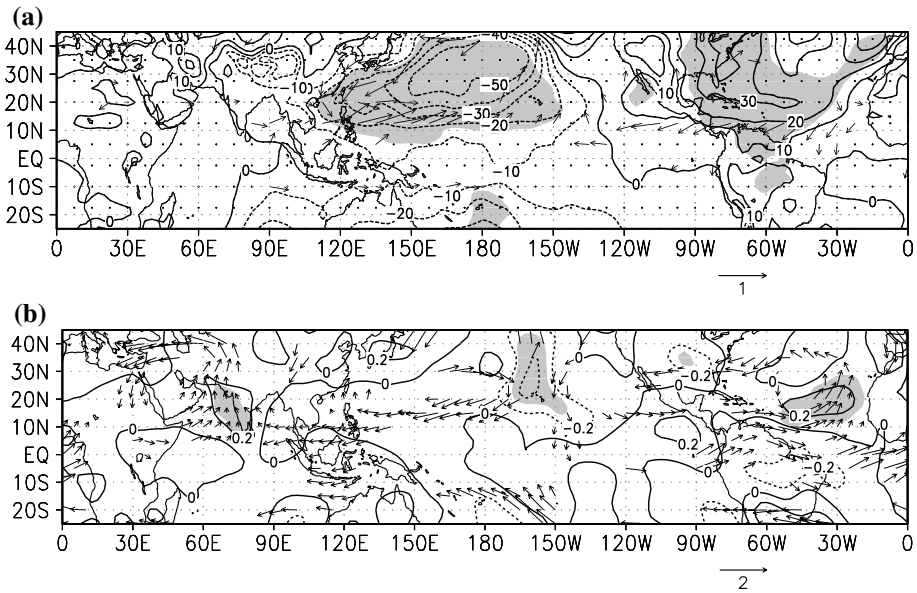

Fig. 9 Regressed **a** 1000 hPa wind (unit: ms^{-1}) and surface level pressures (contour, unit: Pa) and **b** 200 hPa wind (unit: ms^{-1}) and 500 hPa vertical velocity (contour, unit: Pa s^{-1}) against the TNAI during JASO. The *shading* represents the region of 95 % confidence level or higher for the contour. For wind vectors, only regions higher than 90 % confidence level are plotted

question, we conducted a series of numerical experiments using ECHAM4 T42. In a control experiment, the GCM is forced by climatologic annual cycle SST. In the first sensitivity experiment, a negative SST anomaly derived from the regression shown in Fig. 8 in the TNA was added to the climatologic annual cycle SST field. The difference between the sensitivity and control experiments shows the atmospheric response to the specified cold SST anomaly. The numerical result showed that the westerly wind response to the negative SSTA in the tropical Atlantic Ocean cannot penetrate all the way into the tropical western Pacific. The most pronounced low-level wind response is confined in the western Indian Ocean (Fig. 10a). This indicates that TNA forcing alone is not sufficient to directly influence the circulation in the WNP which are shown in Fig. 9.

In the second sensitivity experiment, both the tropical Atlantic and Indian Ocean SST anomalies are specified. As expected, the cold SSTA in NIO suppress local convection. In response to the negative heating anomaly in the NIO, pronounced low-level westerly anomalies appear over the WNP monsoon trough region (Fig. 10b). The westerly anomalies induce anomalous cyclonic shear and a positive relative vorticity anomaly to the north of the maximum zonal wind anomaly (Fig. 10b), leading to an enhanced Ekman pumping and boundary layer convergence in the WNP (Wu et al. 2009, 2010). The enhanced low-level cyclonic vorticity and enhanced boundary moisture convergence further strengthen the WNP monsoon trough. The enhanced monsoon cyclonic vorticity and the weakened vertical shear favor TC genesis over eastern WNP. The numerical model results support the Indian Ocean relaying hypothesis.

In the third sensitive test, a negative SST anomaly derived from the regression shown in Fig. 8 in the Indian Ocean was added to the climatologic annual cycle SST field. The numerical result shows that the Indian Ocean cold SST excites a baroclinic Kelvin wave of the same sign as the cold TNA SST does to the east of Indian Ocean in the tropical Pacific, a Rossby wave of the opposite sign as the cold TNA SST does in the west of the Indian Ocean (Fig. 10c). Similar to the mechanism suggested by Xie et al. (2009) and Wu et al. (2009), a negative heat source in the tropical Indian Ocean induces a first-baroclinic mode Kelvin wave response and thus low-level westerly anomalies to its east, leading to an anomalous cyclone in the WNP.

Comparing Fig. 10 with Fig. 9a, we can find that both the Indian Ocean and TNA cold SST lead a stronger and larger cyclone anomaly than only one's forcing over the WNP, while the cold Indian Ocean triggers an easterly anomaly to its west, which is opposite to the westerly anomaly excited by the cold TNA, leaving little net wind anomalies over the Africa as observed results shown in Fig. 9a.

We also run additional three idealized SSTA experiments with the specified SSTA amplitude being twice as strong as the regressed one. The wind response patterns (not shown) are in general similar to those in Fig. 10, except the wind magnitude is larger. We calculated the GPI field from the ECHAM4 simulations (shown in Fig. 10) and found that a positive GPI anomaly appears over most of the WNP regions when the negative SSTA is specified over the TNA, NIO or both the TNA and NIO. Figure 11 shows averaged GPI values over (10°–20°N, 110°–150°E) from three sensitivity experiments. In response to the cold SSTA

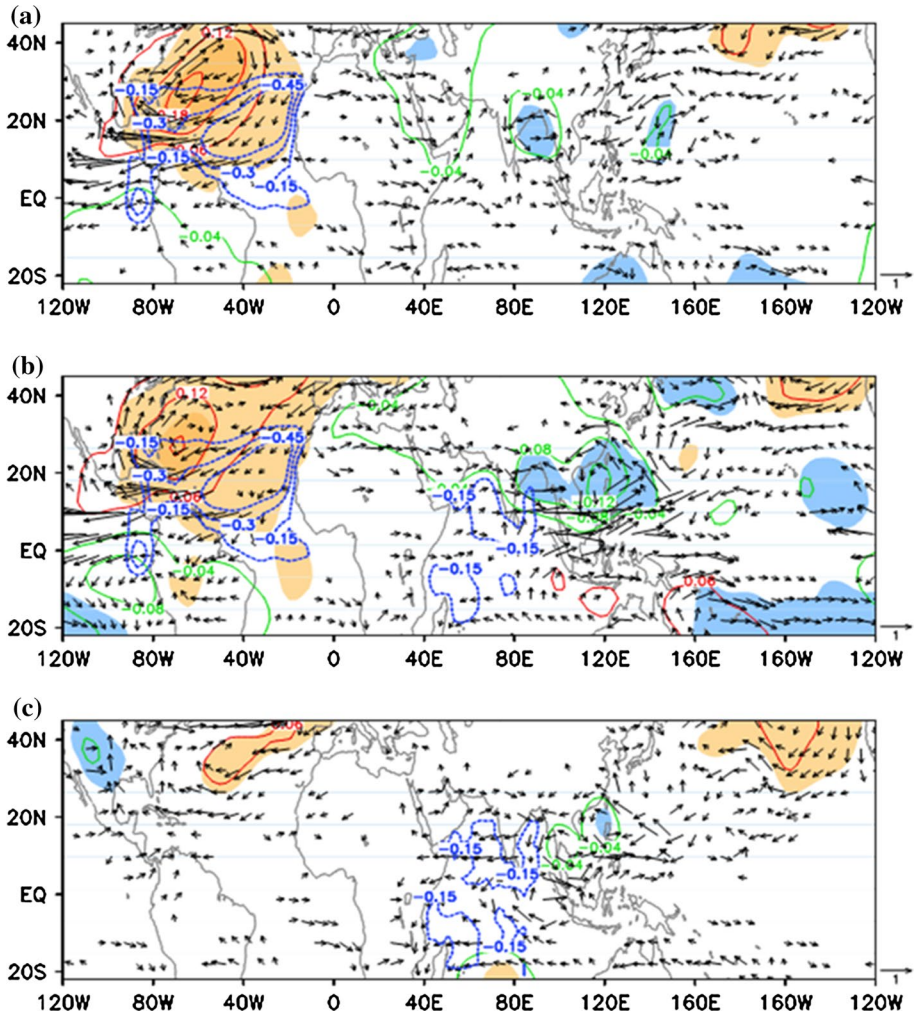

Fig. 10 Atmospheric responses to Atlantic Ocean (**a**), both Atlantic Ocean and Indian Ocean cooling (**b**) and Indian Ocean cooling (**c**) SSTA patterns derived from the regression analysis shown in Fig. 8 from ECHAM model simulation. *Shading* is SLP (unit: Pa), *Vector* is 850 hPa wind (unit: m s^{-1}, only differences exceeding 90 % confident level are shown), *blue dashed* contour is the prescribed SST cooling (unit: °C), *Green* (*red*) contour is 850 hPa stream function (unit: 10^7 m^2 s^{-1})

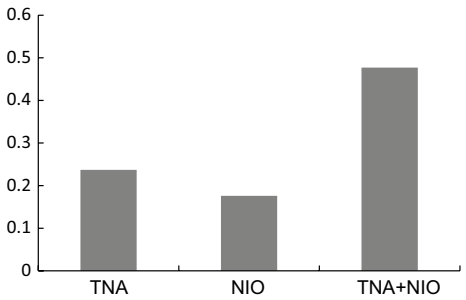

Fig. 11 The area-averaged GPI over a domain (10°–20°N, 110°–150°E) derived from the cases when a cold SSTA is specified over the TNA, NIO, and both the TNA and NIO. The SSTA patterns are same as those shown in Fig. 10

forcing in TNA or/and NIO, area-averaged GPI increases. This implies the occurrence of more frequent TCs in the WNP. The numerical model results are consistent with the observational analysis. The output results of our numerical atmospheric model support the conclusion that the surface cooling or warming in the TNA may, through atmospheric teleconnection, influence the TC genesis probability over the WNP although it cannot directly support the argument that the cold SST over TNA causes the SST cooling over the NIO through the enhanced evaporation by surface wind.

We have shown in Sect. 3 that the overall contribution to the high–low–high longitudinal distribution shown in Fig. 1b arises from environmental relative humidity, relative vorticity and vertical shear. We have further demonstrated in Sect. 4 that the regressed spatial pattern of environmental relative humidity, relative vorticity and vertical shear on TNAI are consistent with that regressed on TCGN. To understand how the relative humidity, relative vorticity and vertical wind shear fields respond to the tropical Atlantic SSTA forcing, we examined the regression patterns of relative vorticity, relative humidity (including temperature and specific humidity), zonal wind and vertical shear fields. It shows that the low level relative vorticity increases over the WNP (Fig. 7a), the mid-level temperature decreases over the equatorial western Pacific and SCS region. The variation of specific humidity is not significant over the WNP (not shown). Our calculations show that the

Table 2 Composite difference of specific humidity (SH) and temperature (T) at 600 hPa during JASO between the high and low TNAI years and the contribution to relative humidity (RH) change by SH difference only and T difference only

	SCS		WWNP	
	SH	T	SH	T
SH or T anomaly	-0.01 gkg^{-1}	-0.33 °C	-0.17 gkg^{-1}	-0.16 °C
Contribution to RH	-0.15	0.73	-2.46	0.31

SCS has a domain of 100°–120°E, 10°–25°N and WWNP has a domain of 120°–140°E, 10°–25°N

relative humidity change is primarily affected by temperature anomaly in the SCS box, while it is mainly affected by specific humidity anomaly over the WWNP box. Table 2 confirms that the temperature contribution to relative humidity change is larger than the specific humidity contribution over the SCS region (0.73 vs. -0.15), while the former is much smaller than the latter over the WWNP region (0.31 vs. -2.46). The change of relative humidity in both the regions is approximately caused by the linear combination of the temperature and specific humidity contributions.

The decrease of mid-level temperature in the SCS is associated with the northerly wind anomaly on the west flank of cyclonic flow response over the WNP to both the TNA and IO SSTA forcing (Figs. 9a, 10b). The decrease of specific humidity in the WWNP, on the other hand, is possibly caused by dry meridional advection near 140E (Fig. 9a). The analysis result above suggests that the tropical Atlantic SSTA affects the anomalous TCGN in the SCS and WWNP through the change of local relative vorticity, temperature and specific humidity and thus relative humidity field.

The anomalous 200-hPa wind field shows a pronounced easterly wind anomaly (Fig. 9b), whereas the 850-hPa wind field shows an opposite pattern, with dominant westerly wind anomalies (similar to Fig. 9a) in the tropical WNP. As demonstrated by the idealized numerical model simulations, the anomalous zonal wind pattern is likely a result of atmospheric responses to both the remote SSTA in the TNA and Indian Ocean. It is interesting to note that the anomalous winds in both the upper and lower troposphere are against the climatologic winds in EWNP. This is why the vertical shear speed decreases significantly in the EWNP (Fig. 7d).

6 Conclusion and discussion

In this study, we analyzed the interannual variation of TCGN in JASO over the WNP and its relationship with global SST anomalies for the period of 1970–2009. It is found that the dominant TCGN mode has a remarkable longitudinal distribution with a high–low–high pattern. The increase of TC genesis frequency is primarily influenced by the TC increase in the eastern WNP and SCS. They explain 42.2 and 23.4 % variance of the TCGN at a 99 % (F test) confidence level, respectively. Given that the longitudinal pattern of GPI resembles that of TCGN, we further identify the quantitative contributions of environmental variables that contribute to such a longitudinal distribution. It is found that the contribution associated with environmental vertical shear is critical for the GPI change in the eastern WNP, while environmental relative humidity is important for the positive and negative GPI anomalies in SCS and the western WNP, respectively. The relative vorticity is important for the positive GPI anomalies in both SCS and EWNP.

The TCGN in the WNP during JASO has a significantly negative correlation with SSTA in the TNA, that is, TC genesis frequency in the WNP increases when the Atlantic SSTA are below normal, and vice versa. The TC number in the colder SSTA years is 5 TC year^{-1} more than that in the warmer SSTA years. A TNA SST index (TNAI) was introduced, and this index is significantly correlated to TCGN in the WNP at a 99 % confidence level.

The longitudinal distribution of TC genesis frequency regressed onto TNAI is similar to that regressed onto the WNP TCGN series. The spatial patterns of regressed environmental variables associated with TNAI resemble those derived based on TCGN in the WNP, implying that the variations of large-scale circulation patterns that affect longitudinal distribution of TC genesis frequency in the WNP are closely related to the remote SSTA forcing over the tropical Atlantic.

We put forth a northern Indian Ocean relaying mechanism through which the tropical Atlantic SSTA can remotely influence the summer monsoon mean circulation in the WNP. In response to a cold SST anomaly in the tropical Atlantic, convective activity is suppressed in situ. This leads to a negative local diabatic heating anomaly. A Gill type Rossby wave atmospheric response with pronounced low (upper) -level easterly (westerly) anomalies appears to the west of the negative SSTA. To the east of the Atlantic cold SSTA, westerly wind anomalies are induced as a Gill type Kelvin-wave response. Because the mean winds are westerlies in boreal summer over NIO, the anomalous westerly could enhance surface evaporation/ocean vertical mixing and lead to SST cooling in northern and equatorial IO. The cold SSTA in NIO further induce anomalous westerlies in the WNP, which enhance cyclonic vorticity and low pressure in the WNP monsoon region. The enhanced monsoon trough in the WNP favor more frequent TC genesis.

The IO relaying effect is further supported by a lagged correlation analysis between SSTA in the TNA and the NIO (Fig. 12). It is found that there is a significant positive correlation between the two, and maximum correlation appears

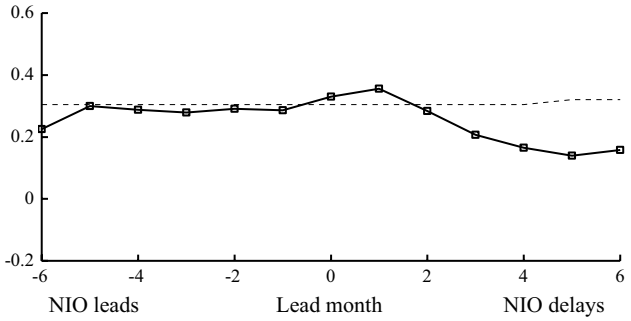

Fig. 12 Cross correlations (1970–2009) between the TNAI during JA and SSTA over the North Indian Ocean (averaged SST over 60°–90°E, 0°–20°N). The *dashed line* indicates a 0.05 significant level

when the TNA SSTA leads the NIO SSTA by 1 month. This indicates that the tropical Atlantic SSTA during JA exert a strong impact on the NIO SSTA. The statistical analysis result is consistent with the ECHAM4 model result that westerly anomalies are induced over the NIO in response to cold SSTA forcing in the TNA, while there is little response in the TNA to cold SSTA forcing over the IO. If allowing the atmosphere influencing the ocean, one would expect the formation of negative SSTA over the NIO due to enhanced surface evaporation. The so–induced SSTA and associated mid-tropospheric cooling in the NIO may further promote circulation change over the WNP. Through this IO relaying effect, SSTA over the TNA in boreal summer exert a remote impact on TC activity in the WNP.

The examination of the GPI parameters shows that low-level westerly and upper-level easterly anomalies weaken the background westerly shear and favor for more frequent TC genesis over the EWNP, where the climatological trade wind is pronounced. Increasing background relative humidity due to the tropospheric cooling favors more frequent TC genesis over the SCS region. The dry meridional advection, on the other hand, might be responsible for the decrease of background relative humidity and TC genesis frequency in the WWNP.

The proposed IO relaying mechanism in this study was purely based on the diagnosis of observational data and atmospheric model simulations. Although it is physically plausible, such a hypothesis requires a further validation with the use of a coupled atmosphere-ocean model. Such a modeling study is currently on-going, and results will be reported elsewhere. The observed longitudinal distribution of GPI within the WNP cannot be reproduced by idealized numerical experiments. The purpose of the numerical experiments in Sect. 4 is to understand how remote SSTA in the TNA and NIO influences circulation anomalies in the WNP. Such an impact must be of large scale, and thus it is difficult to reveal the longitudinal variation of environmental vorticity, humidity and vertical shear fields within the WNP region. Another reason is that the model has a systematic bias in simulating the mean monsoon trough (in both intensity and location) in the WNP. The effect of local SST anomalies is also not included in the above sensitivity experiments. This is why the model is unable to assess regional characteristics of the GPI parameters.

This paper just focuses on the simultaneous effects of SSTA in the Atlantic. By calculating the lead-lag correlation between the NINO3.4 index and TNAI in JA, we found that there is a significant positive correlation between the NINO3.4 index in the preceding winter and TNAI in the concurrent summer. Thus, the cold SSTA in tropical Atlantic might be a result of La Nina forcing in the eastern equatorial Pacific. The connection between the Atlantic and eastern Pacific SSTA is supported by the spectrum analysis result shown in Fig. 5b.

As shown in Fig. 4, the largest correlation appears over the tropical Atlantic. The second largest correlation happens in tropical Indian Ocean, whereas correlation with SSTA in the central equatorial Pacific is much weaker, and not statistically significant. While previous studies (e.g., Zhan et al. 2011) emphasized the role of the tropical Indian Ocean SST on TC genesis in the WNP, the current study suggests that the Indian Ocean SSTA may arise from forcing of SSTA in the tropical Atlantic. We test this hypothesis from two aspects. Firstly from observational point of view, we demonstrate that SST change in the northern Indian Ocean in JASO is significantly correlated with SSTA in the tropical Atlantic (Fig. 8), and that tropical SSTA leads the Indian Ocean SSTA about one month (Fig. 12). Secondly, from modeling point of view, we demonstrate that a cold SSTA in the tropical Atlantic may induce anomalous westerly in NIO in boreal summer, which in turn can cool the ocean surface through enhanced surface evaporation and vertical ocean mixing (because the mean wind is westerly in the region). In short, the relationship between TC genesis over the WNP and SSTA in the tropical Pacific and Indian Ocean has been studied previously, and the relationship between WNP TC genesis and tropical Atlantic SSTA is new and worth studying. A study on the relative contribution of each basin to TCGN variability over the WNP is currently on-going, and results will be reported elsewhere.

Acknowledgments This work was supported by Nation Basic Research Program of China (973 Program) (2015CB453200 and 2012CB955903), NSFC Grant (41130964) and Jiangsu Education Science Foundation (13KJA170002). TL acknowledges the support by NRL Grant N00173-13-1-G902. This is SOEST contribution number 9311, IPRC contribution number 1111, and ESMC 123.

References

Camargo SJ, Emanuel KA, Sobel AH (2007) Use of a genesis potential index to diagnose ENSO effects on tropical cyclone genesis. J Clim 20:4819–4834

Camargo SJ, Wheeler MC, Sobel AH (2009) Diagnosis of the MJO modulation of tropical cyclogenesis using an mpirical index. J Atmos Sci 66:3061–3074

Chan JCL (2000) Tropical cyclone activity over the western North Pacific associated with El Niño and La Niña events. J Clim 13:2960–2972

Chen TC, Wang SY, Yen MC (2006) Interannual variation of the tropical cyclone activity over the western North Pacific. J Clim 19:5709–5720

Chia HH, Ropelewski CE (2002) The interannual variability in the genesis location of tropical cyclones in the northwest Pacific. J Clim 15:2934–2944

Ding H, Keenlyside NS, Latif M (2012) Impact of the equatorial Atlantic on the El Niño Southern oscillation. Clim Dyn 38:1965–1972. doi:10.1007/s00382-011-1097-y

Dong B-W, Sutton RT (2007) Enhancement of ENSO variability by a weakened Atlantic thermohaline circulation in a coupled GCM. J Clim 20:4920–4939

Du Y, Yang L, Xie S-P (2011) Tropical Indian Ocean influence on Northwest Pacific tropical cyclones in Summer following strong El Niño. J Clim 24:315–322

Emanuel KA (1987) The dependence of hurricane intensity on climate. Nature 326:483–485

Emanuel KA (1988) The maximum intensity of hurricanes. J Atmos Sci 45:1143–1155

Emanuel KA, Nolan DS (2004) Tropical cyclone activity and global climate. Amer Meteor Soc 240–241. Reprints, 26th conference on hurricanes and tropical meteorology, Miami, FL

Frank WM, Young GS (2007) The interannual variability of tropical cyclones. Mon Weather Rev 135:3587–3598

Fu B, Li T, Peng M, Weng F (2007) Analysis of tropical cyclone genesis in the western North Pacific for 2000 and 2001. Weather Forecasting 22:763–780

Fu B, Peng M, Li T, Stevens D (2012) Developing versus non-developing disturbances for tropical cyclone formation, part II: western North Pacific. Mon Weather Rev 140:1067–1080

Gill AE (1980) Some simple solutions for heat-induced tropical circulation. Quart J Roy Meteorol Soc 106:447–462

Gray WM (1968) Global view of the origin of tropical disturbances and storms. Mon Weather Rev 96:669–700

Ham YG, Kug JS, Park JY, Jin FF (2013) Sea surface temperature in the north tropical Atlantic as a trigger for El Niño/Southern oscillation events. Nat Geosci 6:112–116

Kalnay E, Kanamitsu M, Kistler R et al (1996) The NECP/NCAR 40-year reanalysis project. Bull Am Meteorol Soc 77(3):437–471

Kushnir Y (1994) Interdecadal variations in North Atlantic sea surface temperature and associated atmospheric conditions. J Clim 7:141–157

Lander MA (1993) Comments on "A GCM simulation of the relationship between tropical storm formation and ENSO". Mon Weather Rev 121:2137–2143

Lau K-H, Lau N-C (1990) Observed structure and propagation characteristics of tropical summertime synoptic-scale disturbances. Mon Weather Rev 118:1888–1913

Li T (2006) Origin of the summertime synoptic-scale wave train in the western North Pacific. J Atmos Sci 63:1093–1102

Li T (2012) Synoptic and climatic aspects of tropical cyclogenesis in western North Pacific. Nova Science Publishers, Inc., Oouchi K, Fudeyasu H (eds) Chap.3, pp.61–94

Li T, Fu B (2006) Tropical cyclogenesis associated with Rossby wave energy dispersion of a pre-existing typhoon. Part I: satellite data analyses. J Atmos Sci 63:1377–1389

Li Z, Yu W, Li T (2013) Bimodal character of cyclone climatology in Bay of Bengal modulated by monsoon seasonal cycle. J Clim 26:1033–1046

Liu K, Chan J (2013) Inactive period of western North Pacific tropical cyclone activity in 1998–2011. J Clim 26:2614–2630

Menkes CE, Lengaigne M, Marchesiello P et al (2012) Comparison of tropical cyclogenesis indices on seasonal to interannual timescales. Clim Dyn 38:301–321

Peng M, Fu B, Li T, Stevens D (2012) Developing versus non-developing disturbances for tropical cyclone formation, part I: North Atlantic. Mon Weather Rev 140:1047–1066

Rayner NA, Parker DE, Horton EB et al (2003) Global analyses of SST, sea ice and night marine air temperature since the late nineteenth century. J Geophys Res 108:4407. doi:10.1029/2002JD002670

Roesch A, Wild M, Gilgen H, Ohmura A (2001) A new snow cover fraction parameterization for the ECHAM4 GCM. Clim Dyn 17:933–946

Rong X, Zhang R, Li T (2010) Impacts of Atlantic SST anomalies on the Indo-East Asian summer monsoon-ENSO relationship. Chin Sci Bull 55:1397–1408

Royer JF, Chauvin F, Timbal B et al (1998) A GCM study of the impact of greenhouse gas increase on the frequency of occurrence of tropical cyclones. Clim Chang 38:307–343

Sutton RT, Hodson DLR (2005) Mechanism of interdecadal thermohaline circulation variability in a coupled ocean-atmosphere GCM. J Clim 18:1117–1135

Sutton RT, Hodson DLR (2007) Climate response to basin-scale warming and cooling of the North Atlantic Ocean. J Clim 20:891–907

Timmermann A, An S-I, Krebs U, Goosse H (2005) ENSO suppression due to weakening of the North Atlantic thermohaline circulation. J Clim 18:3122–3139

Wang B, Chan JCL (2002) How strong ENSO events affect tropical storm activity over the western North Pacific. J Clim 15:1643–1658

Wang BRWu, Li T (2003) Atmosphere-warm ocean interaction and its impact on Asian–Australian monsoon variation. J Clim 16:1195–1211

Wang C, Kucharski F, Barimalala R et al (2009) Teleconnection of the tropical Atlantic to the tropical Indian and Pacific oceans: a review of recent findings. Meteorol Z 18:445–454

Wang X, Wang C, Zhou W (2011) Teleconnected influence of North Atlantic sea surface temperature on the El Niño onset. Clim Dyn 37:663–676

Wu B, Zhou T, Li T (2009) Seasonally evolving dominant interannual variability mode over the East Asia. J Clim 22:2992–3005

Wu B, Li T, Zhou T (2010) Relative contributions of the Indian Ocean and local SST anomalies to the maintenance of the western North Pacific anomalous anticyclone during El Niño decaying summer. J Clim 23:2974–2986

Xie S-P, Hu K, Hafner J et al (2009) Indian Ocean capacitor effect on indo-western Pacific climate during the summer following El Niño. J Clim 22:730–747

Zhan R-F, Wang Y, Lei X-T (2011) Contributions of ENSO and East Indian Ocean SSTA to the interannual variability of Northwest Pacific tropical cyclone frequency. J Clim 24:509–521

Zhao H, Wu L, Wang R (2014) Decadal variations of intense tropical cyclones over the western North Pacific during 1948–2010. Adv Atmos Sci 31:57–65